JOURNAL OF GEOPHYSICAL RESEARCH, VOL. 113, D10207, doi:10.1029/2007JD009190, 2008

Distribution, transport, and deposition of mineral dust in the Southern Ocean and Antarctica: Contribution of major sources

Fuyu Li,[1] Paul Ginoux,[2] and V. Ramaswamy[2]

Received 19 July 2007; revised 7 December 2007; accepted 15 January 2008; published 30 May 2008.

[1] A model-based investigation of the transport, distribution and deposition of mineral dust in the Southern Hemisphere (SH) is performed by using the GFDL Atmospheric Model (AM2). The study represents an attempt to quantify the contribution of the major sources by tagging dust based on its origin. We evaluate the contribution of each source to the emission, distribution, mass burden and deposition of dust in the Southern Ocean and Antarctica, and show that each source produces distinctive meridional transport, vertical distribution, and deposition patterns. The dust in SH originates primarily from Australia (120 Tg a^{-1}), Patagonia (38 Tg a^{-1}) and the inter-hemispheric transport from Northern Hemisphere (31 Tg a^{-1}). A small fraction of it (7 Tg a^{-1}) is transported and deposited in the Southern Ocean and Antarctica, where dust from South America, Australia, and Northern Hemisphere are essentially located in the boundary layer, mid-troposphere, and upper-troposphere, respectively. These three sources contribute to nearly all the dust burden in the Southern Ocean and Antarctica. South America and Australia are the main sources of the dust deposition, but they differ zonally, with each one dominating half of a hemisphere along 120°E–60°W: the half comprising the Atlantic and Indian oceans in the case of the South American dust and the Pacific half in the case of the Australian dust. Our study also indicates a potentially important role of Northern Hemisphere dust, as it appears to be a significant part of the dust burden but contributing little to the dust deposition in Antarctica.

Citation: Li, F., P. Ginoux, and V. Ramaswamy (2008), Distribution, transport, and deposition of mineral dust in the Southern Ocean and Antarctica: Contribution of major sources, *J. Geophys. Res.*, *113*, D10207, doi:10.1029/2007JD009190.

1. Introduction

[2] Mineral dust plays an important role in the Earth system by exerting a significant radiative forcing [*Ramaswamy et al.*, 2001], suppressing precipitation [*Rosenfeld et al.*, 2001], and influencing ozone photochemistry [*Dentener et al.*, 1996]. In the Southern Ocean and Antarctica, dust is of particular interest as an indicator of climate conditions [*Basile et al.*, 1997] and as a fertilizing agent for ocean phytoplankton [*Martin*, 1990].

[3] Dust concentration in Antarctica ice cores and the Southern Ocean marine sediments varies nearly synchronously with temperature and atmospheric CO_2 [e.g., *Petit et al.*, 1999]. It therefore has been suggested to be a good climate indicator and may also likely have played an active role in long-term climate changes by affecting climate variables through radiative feedbacks [*Basile et al.*, 1997]. The radiative effect of dust is exerted through scattering and absorbing solar radiation, and could have been potentially large particularly during glacial periods (e.g., Last Glacial Maximum or LGM) when its observed concentration was a factor of 10 times higher in Antarctica [*Steffensen*, 1997; *Petit et al.*, 1999; *Kohfeld and Harrison*, 2001].

[4] Theoretical studies and in situ observations have shown that dust deposition to the oceans provides nutrients (i.e., iron) and thus acts as a fertilizing agent for ocean phytoplankton in regions with iron deficit such as the Southern Ocean [e.g., *Watson et al.*, 2000; *Fan et al.*, 2006]. Consequently, the change of the Southern Ocean biogeochemical cycle induced by dust deposition could modulate the CO_2 flux between the ocean and atmosphere, further contributing to the change of atmospheric CO_2 and climate [*Martin*, 1990].

[5] Several modeling attempts have been made to study the interaction of dust and past climate, in order to understand the observed increased dust deposition in ice cores during LGM [e.g., *Mahowald et al.*, 1999; *Werner et al.*, 2002; *Mahowald et al.*, 2006]. However, the origin of the dust in the Southern Ocean and Antarctica is still unclear and there is no consensus between models and data. Most of the analyses of the Antarctic ice cores indicate that dust originates essentially from South America (specifically Patagonia) with a small fraction from other sources (e.g., at least 85% of dust in the Vostok ice core is from Patagonia) [*Grousset et al.*, 1992; *Basile et al.*, 1997; *Delmonte et al.*, 2004; *McConnell et al.*, 2007]. However, other studies seem to contradict these results in particular

[1]Program in Atmospheric and Oceanic Sciences, Princeton University, Princeton, New Jersey, USA.
[2]Geophysical Fluid Dynamics Laboratory, NOAA, Princeton, New Jersey, USA.

0148-0227/08/2007JD009190$09.00

concerning the contribution of Australian dust sources. *Gaudichet et al.* [1992] and *Revel-Rolland et al.* [2006] showed that the origin of dust in East Antarctica may change with climate, with a larger contribution from Australia in present climate. A modeling study of dust sources and deposition during the LGM by *Mahowald et al.* [1999] attributes half of dust deposited at Vostok from Patagonia, but with a significant contribution from Australia. *Luo et al.* [2003] showed that, for present-day, the contribution from Australian sources is even higher (70–100% of the dust loading). Another study by *Lunt and Valdes* [2002] showed predominant Patagonian origin of dust deposition (>80%) in Antarctica. Thus there arises a compelling need to determine systematically the contributions from the different sources in high latitude SH for present-day before turning to the past climate. This in turn requires a coherent description of dust emission in SH, its atmospheric transport, and deposition.

[6] In this study, we quantify the contribution of each continental source on the emission, distribution of concentration, mass burden and deposition of dust in the Southern Ocean and Antarctica, by using the state-of-art GFDL Atmospheric General Circulation model. The simulations are performed by tagging dust with respect to its origin, and by nudging the simulated winds with NCEP re-analysis in order to replicate as much as possible the present-day meteorology. The model and methods we used are described in section 2. Section 3 presents the sources for the dust in Southern Ocean and Antarctica (3.1), and the overall budget in these regions (3.2). The distribution of dust near the surface and its vertical profiles are described in section 4. Section 5 discusses the contributions of each principal source to the SH dust distribution (5.1), total atmospheric mass burden (5.2), and deposition (5.3) utilizing a series of simulations that account for dust from each of the principal continental origins. Discussions and conclusions emerging from the study are presented in sections 6 and 7.

2. Model Description

2.1. Model Configuration

[7] The state-of-the-art GFDL Atmospheric General Circulation Model AM2 [GFDL GAMDT, 2004] is used in this study, together with the implementation of a new online dust module. The model has a resolution of 2° latitude × 2.5° longitude with 24 vertical levels (on a η coordinate system), and uses the hydrostatic, finite-volume dynamical core [*Lin*, 2004]. The model is driven by the monthly mean observed sea-surface temperature field. The dynamical fields are "nudged" toward the observations (NCEP re-analysis) using a relaxation method, with the relaxation timescale being 6 h [*Moorthi and Suarez*, 1992]. This procedure ensures that the model's meteorology mimics as best as possible the present-day known patterns. The model results are saved every 24 h for the period from 1979 to 1998. The simulation is initialized with zero atmospheric dust. A 1-year simulation appropriate for the 1979 conditions is performed as part of the spin-up before commencing the 1979–1998 integration.

[8] The dust distribution is simulated in AM2 by solving the continuity equation of its concentration and including the parameterization of dust emission developed by *Ginoux et al.* [2001], turbulent diffusion, convection by convective clouds, advection by the winds, dry deposition and wet deposition (in and below clouds) [*GFDL Global Atmospheric Model Development Team*, 2004]. Five size bins of dust particles are prescribed, with the radii ranging as follows: 0.1–1 μm, 1–2 μm, 2–3 μm, 3–6 μm, and 6–10 μm. The corresponding effective radii are 0.75 μm, 1.5 μm, 2.5 μm, 4.5 μm, and 8 μm, respectively. The mass fraction is 10%; the density is 2500 kg m^{-3} for the dust in the smallest size bin (0.1–1 μm). For the other four bins, the mass fractions are all 22.5% with a dust density of 2650 kg m^{-3}.

2.2. Dust Emission

[9] We use the emission scheme of *Ginoux et al.* [2001] where the dust emission flux F_p is calculated as follows:

$$F_p = CSs_p u_{10\mathrm{m}}^2 (u_{10\mathrm{m}} - u_t) \text{ if } u_{10\mathrm{m}} > u_t$$
$$F_p = 0 \qquad \text{otherwise,} \tag{1}$$

where C is a dimensional factor, S is the source function determined empirically and based on topographical map over bare grounds, u_{10m} is the horizontal wind speed at 10 m, u_t is the threshold velocity for dust emission, and s_p is the fraction of each size class. C and u_t can be specified empirically in certain situations. Neither is well-known on the scale of global models. Most models use different values of these two parameters, and these are often chosen so that the model dust distribution matches the available observations. Global emission is sensitive to the data set used and the region used to constrain the model, in addition to the physics of the model [*Cakmur et al.*, 2006]. Following the method used by *Ginoux et al.* [2001], we have used the dust concentration data [*Prospero*, 1996] to constrain C and u_t. A reasonable agreement is achieved with the values of C = 1 μg s^2 m^{-5} and u_t = 0 m s^{-1}. As other choices of the values of these two parameters can potentially provide similar agreement, we have performed a sensitivity study about these two parameters and discuss how these affect our results in section 6.

[10] Dust emission can only occur where the vegetation cover is low and sparse. *Ginoux et al.* [2001] used the vegetation data sets derived from the Advanced Very High Resolution Radiometer (AVHRR) data [*DeFries and Townshend*, 1994] to estimate the dust emission. Within the non-vegetated areas, preferential dust sources (e.g., ephemeral lakes) are taken into account by the source function S, which captures most of the hot spots identified, for example, by *Prospero et al.* [2002] using the frequency of dusty days retrieved from the Total Ozone Mapping Spectrometer (TOMS) data. Thus the *Ginoux et al.* [2001] formulation is adopted for the present study.

[11] It should be noted that the validation of dust sources in the southern hemisphere is particularly difficult when using TOMS data, as dust plumes are generally accompanied by clouds and seem to be traveling at low altitudes [*Gassó and Stein*, 2007]. Indeed, *Torres et al.* [2002] have shown that a major uncertainty in TOMS retrievals is the sub-pixel cloud contamination, and also that there is a reduction of sensitivity when aerosols are in the boundary layer. With the emergence of new satellite instruments which can provide aerosol information over bright surfaces

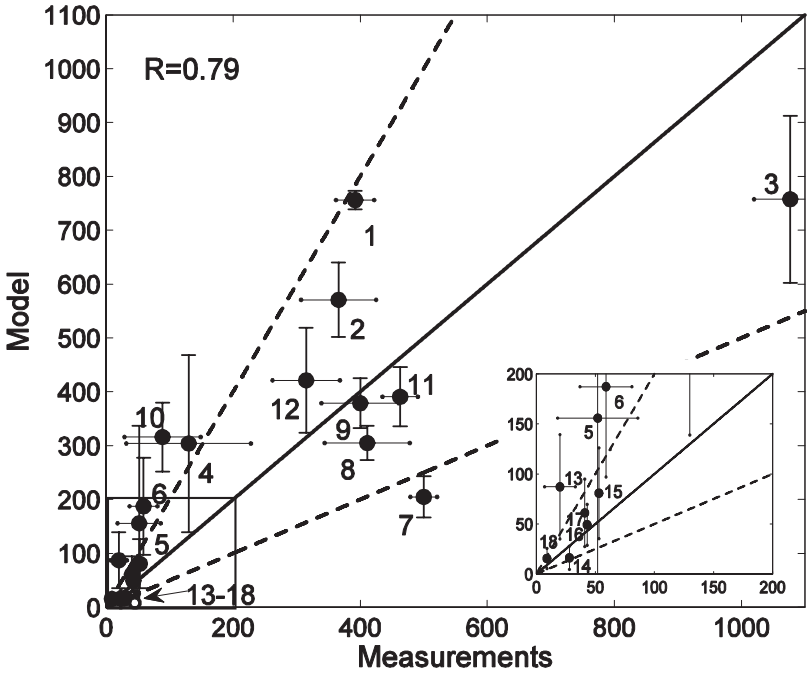

Figure 1. Comparison of simulated and observed ^{222}Rn concentrations (mBq m^{-3}), at 18 locations in the Southern Hemisphere. The vertical bar indicates the standard deviation of the model simulations, and horizontal bar is the uncertainties from measurements. The range smaller than 200 mBq m^{-3} is enlarged in the bottom-right box for easy comprehension. Information on the locations of the sites is described in Table 1.

and high resolution, such as MODIS deep blue retrievals by *Hsu et al.* [2004], it may become possible to better characterize dust sources and their emission in the future.

2.3. Dust Transport

[12] Mineral dust is transported in the atmosphere by advection, convection, and turbulent diffusion; these are described in detail by *GFDL GAMDT* [2004]. Briefly, the advection is calculated by $-\vec{V}\,\nabla\psi$, where ψ is the dust concentration and $\vec{V} = (U, V, \Omega)$ are wind components. The wind velocities in AM2 are obtained by using the finite-volume scheme of *Lin* [2004], and are nudged toward the observations (NCEP re-analysis) using the following relaxation method

$$\frac{\partial \vec{V}}{\partial t}\Big|_{nudge} = \frac{\vec{V}^{NCEP} - \vec{V}^{AM2}}{\tau + \Delta t}, \tag{2}$$

where τ = 21600 s and Δt = 1200 s. The subgrid-scale vertical mixing is parameterized using $\nabla \cdot (K\nabla\psi)$, where the eddy diffusion coefficients K(m^2 s^{-1}) are predicted in the model. The influence of convection on the dust distribution is parameterized through large scale and deep convection [*GFDL GAMDT*, 2004].

[13] This study focuses on the dust cycle in the Southern Ocean and Antarctica. In situ observations of dust are sparse in this region, and satellite products do not seem to provide adequate information to validate dust transport in high latitude SH. As an alternative to validate our transport scheme, we have simulated ^{222}Rn which has been measured at many different locations in SH. The emission of ^{222}Rn is constant over land ($\sim$ 1 atoms cm^{-2} s^{-1}), and its e-folding lifetime is $\sim$5.5 days, similar to that of dust. Figure 1 shows the comparison between the simulated ^{222}Rn concentrations (mBq m^{-3}), and those observed at 18 locations in SH (Table 1) using data from *Ramonet et al.* [1996], *Pereira et al.* [1988] and *Polian et al.* [1986]. The data from the last two studies are annual-mean values, and these are compared with climatological annual-mean results from our simulation. Although *Ramonet et al.* [1996] data corresponds to hourly values and the temporal resolution of our model diagnostics is monthly mean, they do offer an opportunity to test our transport scheme by comparing the ^{222}Rn concentration at different altitudes and locations all around South America.

[14] The correlation coefficient between simulated and observed ^{222}Rn concentration is $\sim$ 0.8. The model captures most of the latitudinal and vertical gradients of ^{222}Rn, although it tends to overestimate the low concentration values.

2.4. Removal Processes

[15] Dust in the atmosphere is removed by two types of processes: dry deposition and wet deposition. Dry deposition includes gravitational settling and turbulent transfer to the surface. The total dry deposition flux is calculated using $D = \psi \cdot V_d$, where the units of D is kgm^{-2} s^{-1}, ψ is the dust concentration, and V_d is the dry deposition velocity. V_d is expressed as

$$V_d = V_g + \frac{1}{(R_a + R_s) + R_a R_s V_g}, \tag{3}$$

Table 1. Radon 222 Concentration Measurements[a]

Location #	Latitude	Longitude	Altitude, m	Observed ^{222}Rn, mBqm^{-3}	Simulated ^{222}Rn, mBqm^{-3}
1	5.1°S	81.3°W	10973	392	756
2	10.1°S	78.2°W	10960	366	571
3	13.9°S	76.4°W	10180	1077	757
4	17.4°S	74.1°W	11057	130	304
5	35.6°S	71.5°W	11033	52	156
6	29.3°S	50.3°W	7780	59	187
7	20.9°S	42.0°W	11033	500	205
8	16.0°S	39.7°W	11007	411	305
9	13.9°S	38.5°W	4973	400	379
10	11.7°S	38.2°W	8870	89	316
11	8.7°S	37.9°W	11000	463	391
12	2.9°S	37.5°W	10530	315	421
13	62°S	58°W	surface	20	87
14	68°S	140°E	surface	28	16
15	56°S	50°E	surface	53	81
16	49°S	69°E	surface	43	49
17	38°S	77°E	surface	41	61
18	68°S	63°E	surface	9	15

[a]Measurements sampled in locations 1–12 are from *Ramonet et al.* [1996], 13 is from *Pereira et al.* [1988], and 14–18 are from *Polian et al.* [1986].

where V_g is the gravitational settling velocity determined by the density and diameter of dust particles, and the viscosity coefficient of air. R_a is the aerodynamic resistance above the surface and R_s is the surface resistance [*Slinn*, 1982].

[16] Wet deposition process includes rainout and washout of dust in and below cloud. In this study, wet deposition (or scavenging) of dust is treated separately for large scale (ls) and convective (cv) rain. The deposition flux is also directly proportional to the local concentration in the case of wet deposition, given by $W = \Gamma\psi$, where Γ (s^{-1}) is the wet scavenging coefficient. A parameterization similar to *Boucher et al.* [2002] is applied to estimate the wet scavenging coefficient Γ.

[17] The below cloud scavenging coefficient is $\Gamma_{bc} = \Gamma_{bc}^{ls} + \Gamma_{bc}^{cv}$ with

$$\Gamma_{bc}^{ls,cv} = \frac{3}{4}\left(\frac{P_{rain}\cdot\alpha_{rain}}{R_{rain}\cdot\rho_{H_2O}} + \frac{P_{snow}\cdot\alpha_{snow}}{R_{snow}\cdot\rho_{snow}}\right), \quad (4)$$

where P_{rain} and P_{snow} are the precipitation fluxes (kgm^{-2} s^{-1}) as defined in AM2, α is the efficiency with which aerosols are collected by raindrop and snow with α_{rain} = 0.001 and α_{snow} = 0.001, R is the radius of cloud droplets with R_{rain} = 0.001 m and R_{snow} = 0.001 m, ρ is density with ρ_{H2O} = 1000 kgm^{-3} and ρ_{snow} = 500 kgm^{-3}.

[18] For the in cloud scavenging,

$$\Gamma = 1 - \exp(-\beta\cdot a\cdot f), \quad (5)$$

with

$$\beta = \frac{P_{rain}^{k+1} - P_{rain}^{k} + P_{snow}^{k+1} - P_{snow}^{k}}{\Delta z\cdot w\cdot\rho}. \quad (6)$$

[19] The liquid water content w $\left(=\frac{liquid(kg)}{air(kg)}\right)$ is as follows: w^{ls} = 0.005 and w^{cv} = 0.001. The air density ρ is calculated from the hydrostatic approximation. Δz is the model layer thickness. P^k is the precipitation flux at model level k and the scavenging factor f (= 0.4) defines the fraction of aerosol incorporated in the raindrops and snow.

3. Budget in SH

3.1. Emission for SH sources

[20] The distribution of the 20-year annual mean dust emission, using the equations in section 2, is shown in Figure 2. The global emission is 2323 Tg a^{-1}, varying from 2220 Tg a^{-1} in 1982 to 2450 Tg a^{-1} in 1990. The largest contribution to total dust emission (~90%) is from Northern Hemisphere, mostly in North Africa. Only ~10% is emitted from the three continents in SH. These results are within the range of previous model estimates (1000–3000 Tg a^{-1}) but toward the high end, higher than the estimates in studies that employed the same emission scheme [e.g., *Ginoux et al.*, 2001; *Luo et al.*, 2003]. This may be due to the wind intensities between models, since these are the major parameters differing from the other studies. Further inter-model comparison and sensitivity analyses would be necessary to identify the source of the differences as the emission strongly depends on the meteorological data sets and source parameterizations used in the models; note there are still large uncertainties in data sets [*Luo et al.*, 2003, 2004].

[21] In this work, the global dust sources are divided into four major regions, as indicated in the four boxes in Figure 2, referred as (1) SAM for all the dust sources in South America, (2) SAF for those in South Africa, (3) AUS for those in Australia, and (4) NHE for those in Northern Hemisphere. We summarize the simulated annual mean emission of these sources in Table 2.

3.1.1. Australia

[22] The interior of the Australia continent is characterized by arid condition due to the low precipitation rate (<1 mm/d). More than half of the land is occupied by desert and semidesert, and includes dune fields and playa lakes

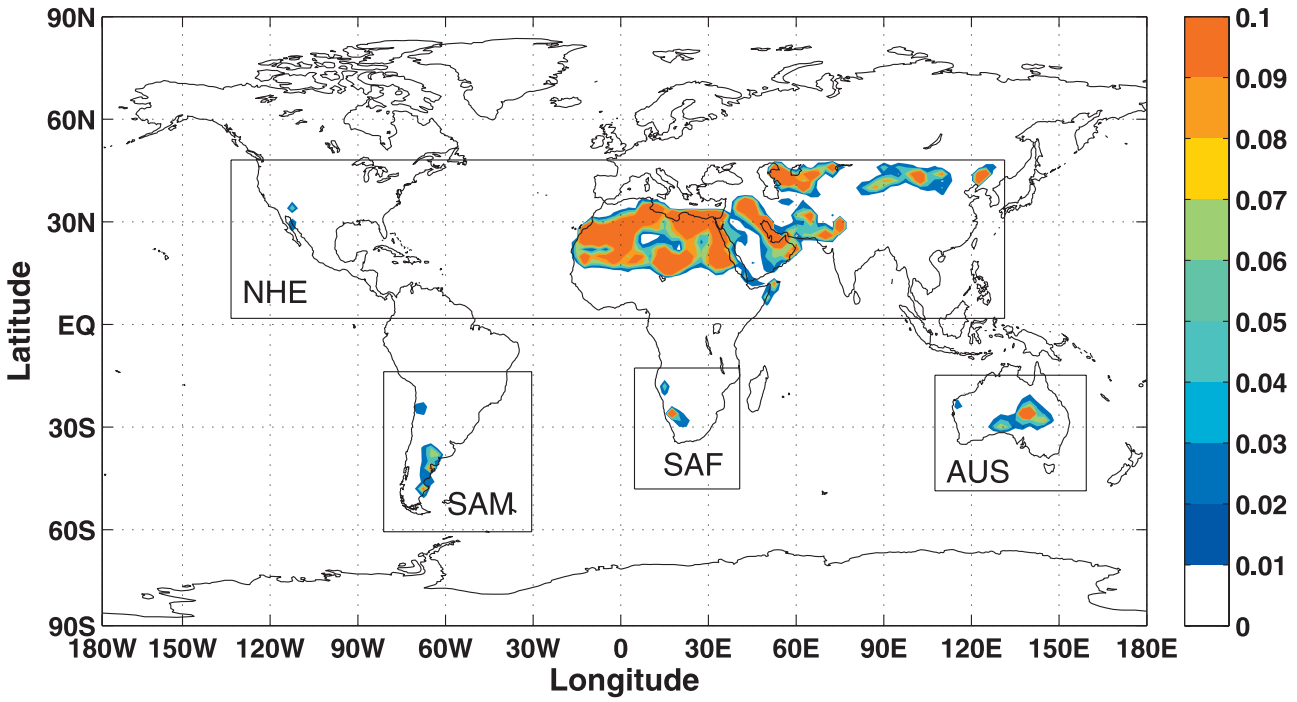

Figure 2. Global distribution of annual dust emission, averaged over 20 years (1979–1998) in units of $kgm^{-2}\ a^{-1}$. The four boxes labeled by NHE, SAM, SAF, and AUS indicate the four major source regions defined in section 3.1.

which are potential dust sources. Persistent dust activities are observed at two locations: the Great Artesian Basin in central Australia and the Murray-Darling Basin in southeastern Australia [*McTainsh*, 1998; *Prospero et al.*, 2002].

[23] The AM2 simulated annual dust emission in AUS, averaged over the 20 years, is $\sim 120 \pm 8.4$ Tg a^{-1}, which is slightly less than the emission (132 Tg a^{-1}) simulated by *Luo et al.* [2003]. As can be seen in Figure 2, the highest dust emission appears in central and eastern Australia at the two basins described above, concurring with these observations. Monthly variation of simulated emission indicates a high dust production in austral summer starting in October and ending in March, in agreement with satellite data [*Prospero et al.*, 2002] and with observations of dust storm frequency in southeastern Australia [*McTainsh and Lynch*, 1996].

3.1.2. South America

[24] High dust production simulated by AM2 is mostly seen in four regions in South America (Figure 2), similar to the observed pattern [*Prospero et al.*, 2002]. These hot spots are (1) Bolivian Altiplano, an elevated intermountain basin centered around ~15°S, (2) the Atacama Desert of Chile roughly between 20° and 30°S, which is known as the world driest region located between the Andes mountains and coastal mountains, (3) a small region in western Argentina (~32°S) along the eastern flanks of the Andes, and (4) Patagonia, which is on the lee side of the Andes between 35°S and 50°S characterized by dry and largely barren land with great saline areas, sandy deserts, and semiarid regions covered with shrubs.

[25] The total emission in South America is $\sim 50 \pm 3.0$ Tg a^{-1}, which is second to the AUS annual emission rate. The simulated dust emissions out of the Bolivian Altiplano and western Argentina are small. The source located in the Atacama Desert contributes ~1/4 of total emission in South America, with an annual emission rate of ~13 Tg a^{-1}. The largest source in South America is Patagonia with an annual emission of ~38 Tg a^{-1}, accounting for >70% of the total emission in South America, much larger than the three other sources. This result is in agreement with the value of 30 Tg a^{-1} of Patagonian dust deposition in the South Atlantic, as estimated by *Gaiero et al.* [2003].

3.1.3. South Africa

[26] The two major sources in South Africa are the Makgadikgadi Pans in Botswana and Etosha Pan Basin. The simulated annual emission is $\sim 34 \pm 2.1$ Tg a^{-1}, only a

Table 2. Annual Mean Dust Emission (Tg a^{-1}) From Global Principal Sources, and the Dust Burden (Tg*10^{-3}) and Fractional Contribution (Percentage) From These Sources in the Southern Ocean and Antarctica

	SAM	AUS	SAF	NHE
Annual emission (source regions)	50	120	34	2119
Burden (Southern Ocean)	40.4 (~39%)	34.9 (~34%)	5.0 (~5%)	22.7 (~22%)
Burden (Antarctica)	1.17 (~19%)	2.07 (~34%)	0.36 (~6%)	2.57 (~42%)

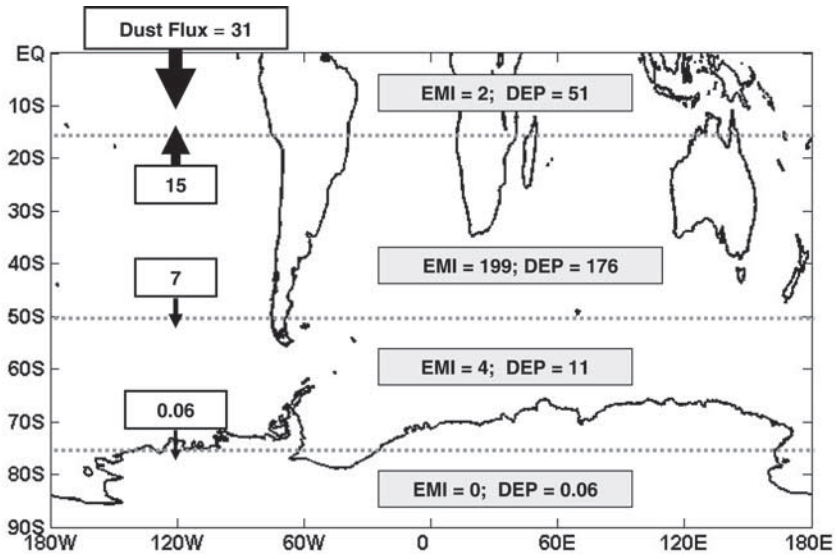

Figure 3. Dust budget in SH low-latitude region (EQ-15S), source region (15S-50S), the Southern Ocean (50S-75S), inland Antarctica (75S-90S). Dust flux, emission (EMI), and deposition (DEP) are all in units of Tg a^{-1}.

quarter of the emission in Australia. Monthly emission stays high from July to January and is lowest during the austral winter. This is consistent with the model study by *Mahowald et al.* [2003]. One point to note is that the results underestimate South African emissions as the Botswana pan is not properly included due to the land cover data set we use in this study.

3.2. Dust Budget in SH

[27] Figure 3 illustrates the dust budget in different portions of the SH, chosen to better understand the dust distribution as it is transported away from the source regions. The 4 regions thus framed are: SH tropical region (EQ-15°S), source region (15°S–50°S), the Southern Ocean (50°S–75°S), inland Antarctica (75°S–90°S).

[28] The global annual mean dust removal in SH is 238 ± 12 Tg a^{-1}, nearly 10–20 % higher than the emission (205 ± 10 Tg a^{-1}). This deficit between emission and removal in SH is balanced by the dust transport across the equator from Northern Hemisphere, ~31 ± 4 Tg a^{-1}, predominantly from North Africa.

[29] The SH tropical region is essentially a sink for the SH dust, with an annual mean deposition of about 51 Tg a^{-1} while the local mean emission is only 2 Tg a^{-1}. The influx of dust in this region is coming from both sides, 15 Tg a^{-1} from SH subtropical source regions and 31 Tg a^{-1} inter-hemispheric transport from Northern Hemisphere.

[30] The source regions between 15° S and 50° S account for nearly all the emission in SH (~199 Tg a^{-1}). 89% of it is deposited back to the surface in this region. Most of the rest dust is exported into the tropical region (15 Tg a^{-1}); the dust transported to the Southern Ocean (7 Tg a^{-1}) represents ~31% of total outflow from the region which is only ~3% of the total dust emitted in the SH.

[31] Most of the dust transported to the Southern Ocean ends up being removed there, with 7 Tg a^{-1} across 50° S but only a tiny fraction (0.06 Tg a^{-1}) gets into inland Antarctica. The total removal in the Southern Ocean (11 Tg a^{-1}) is balanced by the influx from the source region (7 Tg a^{-1}) and local emission in southern end of South America (4 Tg a^{-1}). In Antarctica, there is no dust emission and the mass of dust removed annually (0.06 Tg a^{-1}) is compensated by the mass transported into this region.

4. Distribution in SH

4.1. Surface Dust Concentration

[32] As a direct indication of global dust distribution and a useful parameter to compare with field measurements, the simulated annual mean (1979–1998) dust concentration at the surface is illustrated in Figure 4a. In NH, there is a "dust belt" with concentrations greater than 10 μ gm^{-3}, extending from the Caribbean to East Asia. In the SH, concentrations are much less and only found directly over the three major sources.

[33] Figure 4b shows the comparison of simulated and observed annual mean concentrations. The dust concentration is compared at 20 sites with the data provided by University of Miami [*Prospero*, 1996]. The location of each site is indicated in Figure 4a. Most of the 9 sites in SH (circles and squares) are located in South Pacific Ocean downwind of Australia. There are two sites along the Antarctic coast, Mawson (67.60° S, 62.50° E) in the eastern part and Palmer Station (64.77° S, 64.05° W) in the western part, which are labeled as 7 and 8, respectively, in Figure 4. The dusty stations with values greater than 2 μ gm^{-3} are all in the NH. The highest concentration measured in SH (~ 1 μ gm^{-3}) is at Cape Grim (3), which is located near the coast of the Australian continent downwind of dust source area. Most SH stations are remotely located from source regions with much lower concentrations (0.1 – 0.4 μ gm^{-3}). The correlation coefficient between simulated and observed concentrations is 0.98. The model generally predicts surface dust concentration within a factor of 2 with values ranging

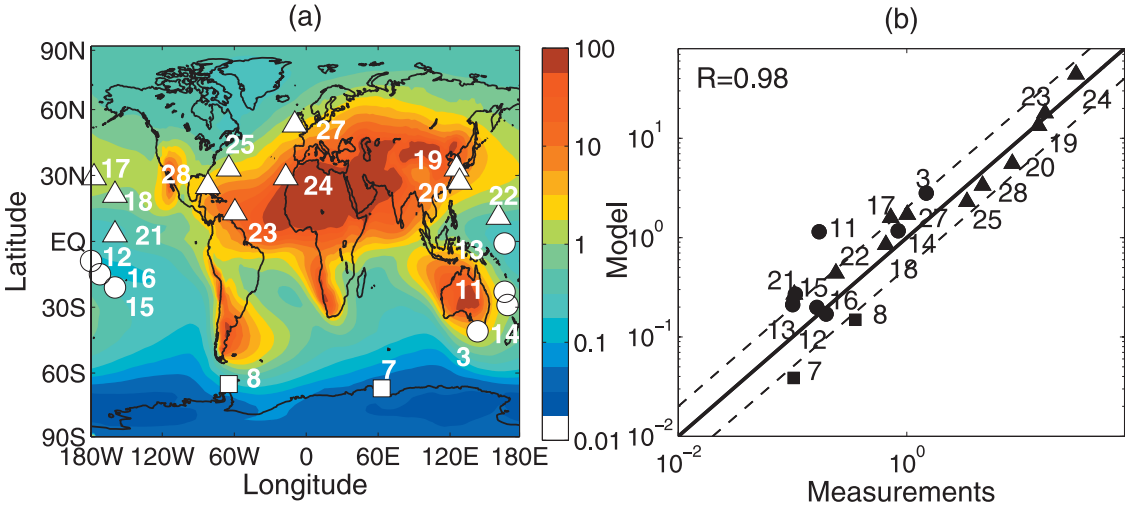

Figure 4. (a) AM2 simulated annual dust concentration at the surface (1979-1998), in units of μ gm^{-3}, with the locations of 20 sites operated by the University of Miami indicated by symbols. (b) Comparison of annual mean dust concentration, simulated and observed in 20 sites in 1988, in units of μ gm^{-3}. The dashed lines are factor of 2 lines. In both (a) and (b), the two sites in Antarctica are shown in squares. The other SH sites are indicated by circles and NH sites are indicated by triangles.

from 0.1 to 30 μ gm^{-3}. The results do not appear to have the systematic bias found in the model results over the Pacific presented by *Ginoux et al.* [2001]. However, the present model underestimates the annual dust concentration in Antarctica by a factor of 3 (Figure 4b).

[34] The comparisons of the monthly mean surface concentrations are shown in Figure 5a and 5b for Mawson and Palmer station, respectively. Different seasonal cycles were observed at the two sites and the model is within one standard deviation of the data, except for June at Mawson. For each month when the model is biased low, the observed standard deviation is particularly important. This indicates that the discrepancy of a factor of 3 in Figure 4b may be attributable to the large interannual variability of the observations. Further analysis of the variation of local conditions near the source regions, such as soil moisture, is needed to better understand the discrepancy.

4.2. Vertical Distribution

[35] In high latitude regions especially in Antarctica, the observations of dust concentration at surface level may differ, with respect to the concentration and seasonal variability, from that higher up in the atmosphere, due to the strong thermal stability of the boundary layer [*Genthon*, 1992]. It is thus also of interest to evaluate the vertical profile of dust in the Southern Ocean and Antarctica in

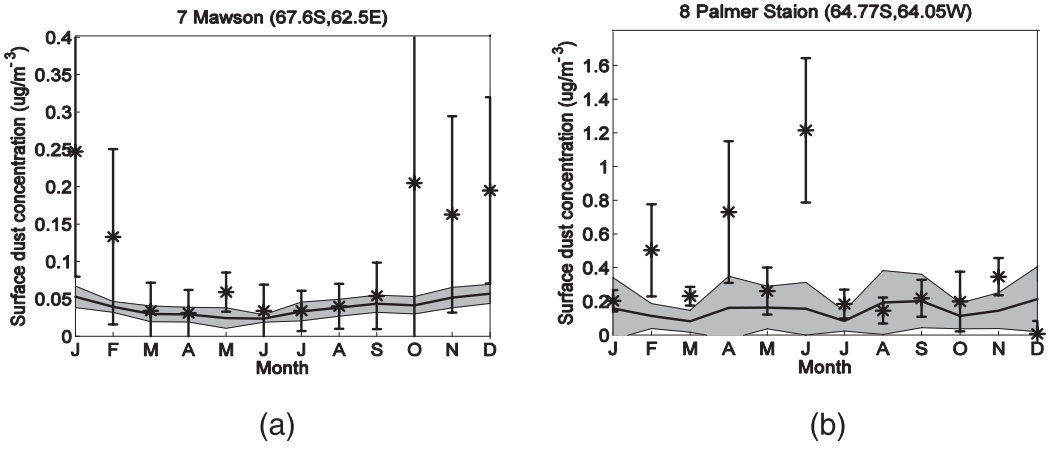

Figure 5. Simulated (solid line) and observed (stars) monthly mean dust concentration (μ gm^{-3}) at the surface at two sites in Antarctica: (a) Mawson (67.60° S, 62.50°E) and (b) Palmer Station (64.77°S, 64.05°W). The vertical bar and shading are the two standard deviations of the simulated and observed concentrations, respectively.

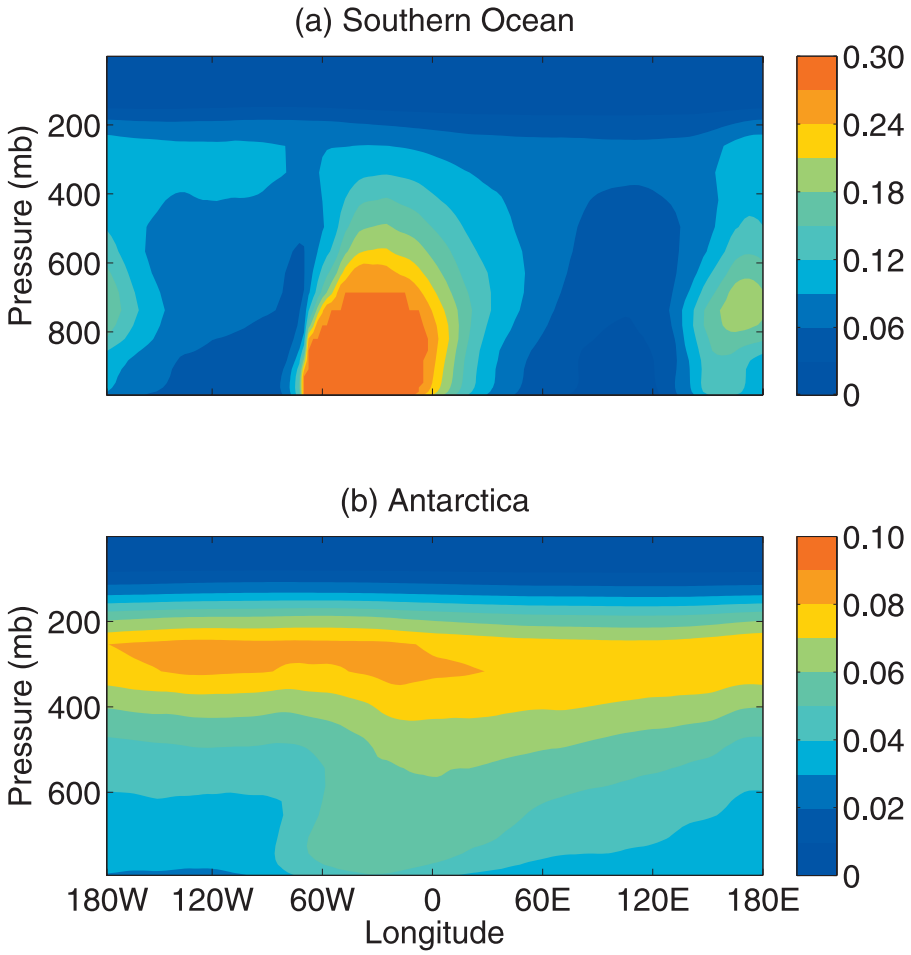

Figure 6. Meridional mean of the vertical distribution of annual dust concentration (μ gm^{-3}) in (a) the Southern Ocean, averaged between 50°S and 75°S, and (b) Antarctica, averaged between 75° and 90°S.

addition to the surface measurements to better understand the dust distribution patterns.

[36] The vertical distribution of dust in the lower troposphere (Figures 6a–6b) indicates two distinct peaks in the Southern Ocean, giving way to one near the pole (Antarctica); this is in contrast to the three dust maxima near the surface corresponding to the three major continents (Figure 4a). The two peaks in Southern Ocean are at 60°–0°W and 160°–180°E which are close, respectively, to the longitudinal locations of South America and Australia but shifted ~30° eastward. Among the two peaks in the Southern Ocean, the maximum dust concentration closer to Australia is located higher up between 800 mb to 600 mb, which is different from the one close to South America. In the lower troposphere, the dust concentration is relatively large in the 60°–0°W region, but is smaller in the other regions. This has an important implication for long range transport as explained later. In Antarctica, the maximum dust concentration is located in the upper troposphere, near the tropopause between 400–200 mb. As discussed previously, the dust concentrations decrease rapidly from the source regions and toward Antarctica. This is apparent in the near total removal of the dust loading contained in the 60°–0°W region from Figure 6a (the Southern Ocean) and Figure 6b (Antarctica). Near the tropopause, the decrease is much less (~20%), suggesting a smaller deposition rate in Antarctica.

5. Contributions From Individual Sources

[37] In order to evaluate the contribution of the individual sources to the dust distribution and removal over the Southern Ocean and Antarctica, we perform a set of simulations in which all sources but one are successively active. The four source regions are designated SAM, SAF, AUS and NHE, respectively, denoting South America, Southern Africa, Australia and Northern Hemisphere as a whole. A particular diagnostic field, X, from a source i is calculated as

$$X(i) = X_{TOT} - X^{off}(i), \tag{7}$$

where X_{TOT} is the result with all sources actives as analyzed in the previous section, and X^{off} (i) corresponds to the simulation with the particular source i turned off.

5.1. Dust Vertical Profile

[38] The vertical profiles of the meridional concentration of dust from each of the four sources are illustrated in Figure 7 for the Southern Ocean (a–d) and Antarctica (e–h),

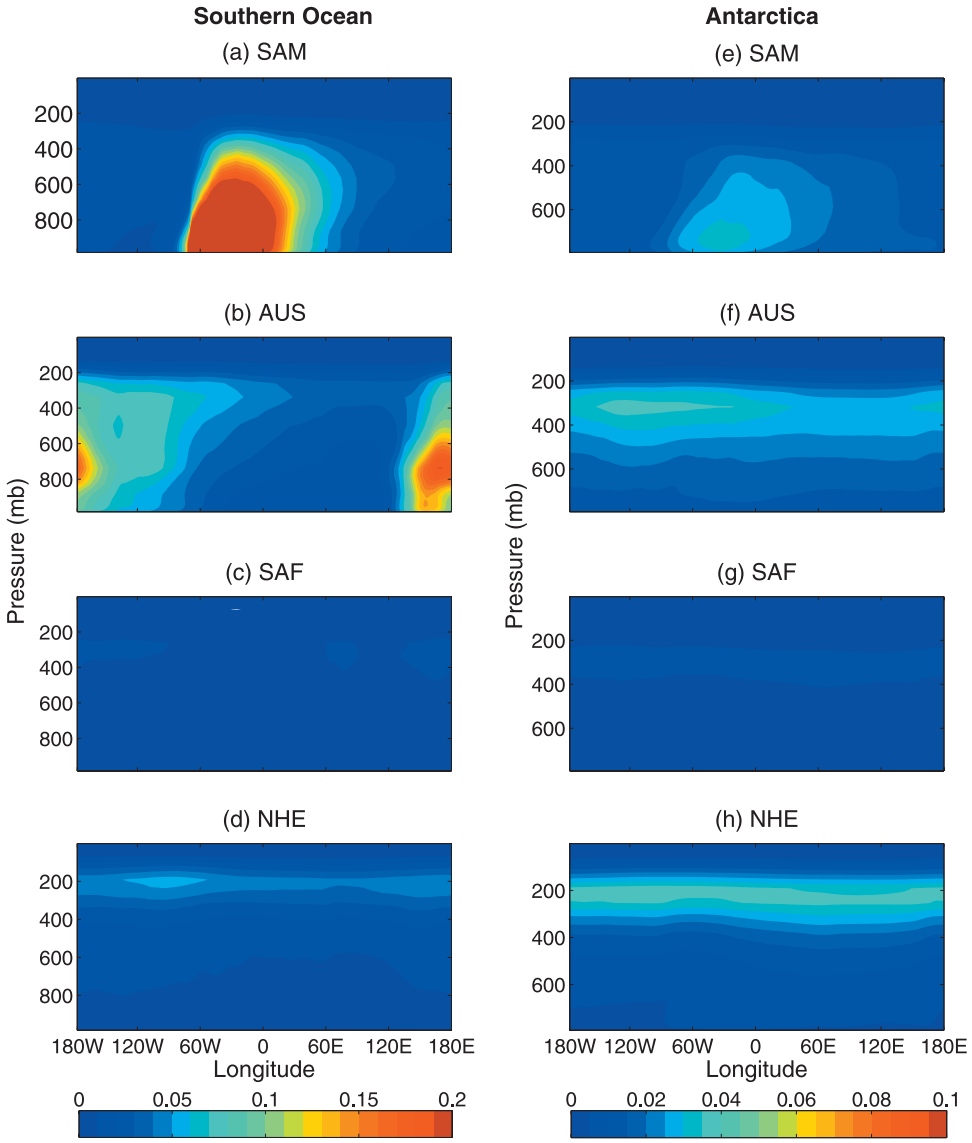

Figure 7. Meridional mean of the vertical distribution of annual dust concentration over the Southern Ocean from (a) SAM, (b) AUS, (c) SAF, and (d) NHE, and over Antarctica from (e) SAM, (f) AUS, (g) SAF, and (h) NHE, in units of μ gm^{-3}.

respectively. Generally, in SH high latitude regions, mineral dust is distributed throughout the troposphere, but different levels are dominated by dust from different sources.

[39] Figures 7a–7b show that the two maxima of dust concentration over the Southern Ocean, as shown in Figure 6, can be attributed to SAM for the one located between 60°–0°W and AUS for the other located between 120°E–160°W. They also reveal that in the Southern Ocean, dust from SAM is essentially seen in the boundary layer, while dust from AUS is concentrated in the free troposphere. The meridional transport of SAM and AUS dust can be inferred from the comparison between Figures 7a–7b and 7e–7f, which indicate that dust from AUS is moved rapidly by the westerly winds in the free troposphere, while dust from SAM stays for the most part in the boundary layer. This difference between the SAM and AUS dust affects their respective long range transport.

[40] The distinctive vertical profiles of dust concentration from SAM and AUS (Figure 7), early in their transport pathways to polar region, may be partially due to the presence of mountains downwind of the source region in Australia. In contrast, the Andes mountains in South America are located upwind. Furthermore, strong wind episodes observed in Patagonia are usually related to the displacement of low pressure systems from the Pacific to the Atlantic Ocean through the Drake Passage. The direction of dust plumes over the Atlantic is controlled by the relative position of these low pressure systems and the South Atlantic semi-permanent anticyclone off the coast of the southern part of Brazil [*Labraga*, 1994]. This anticyclone

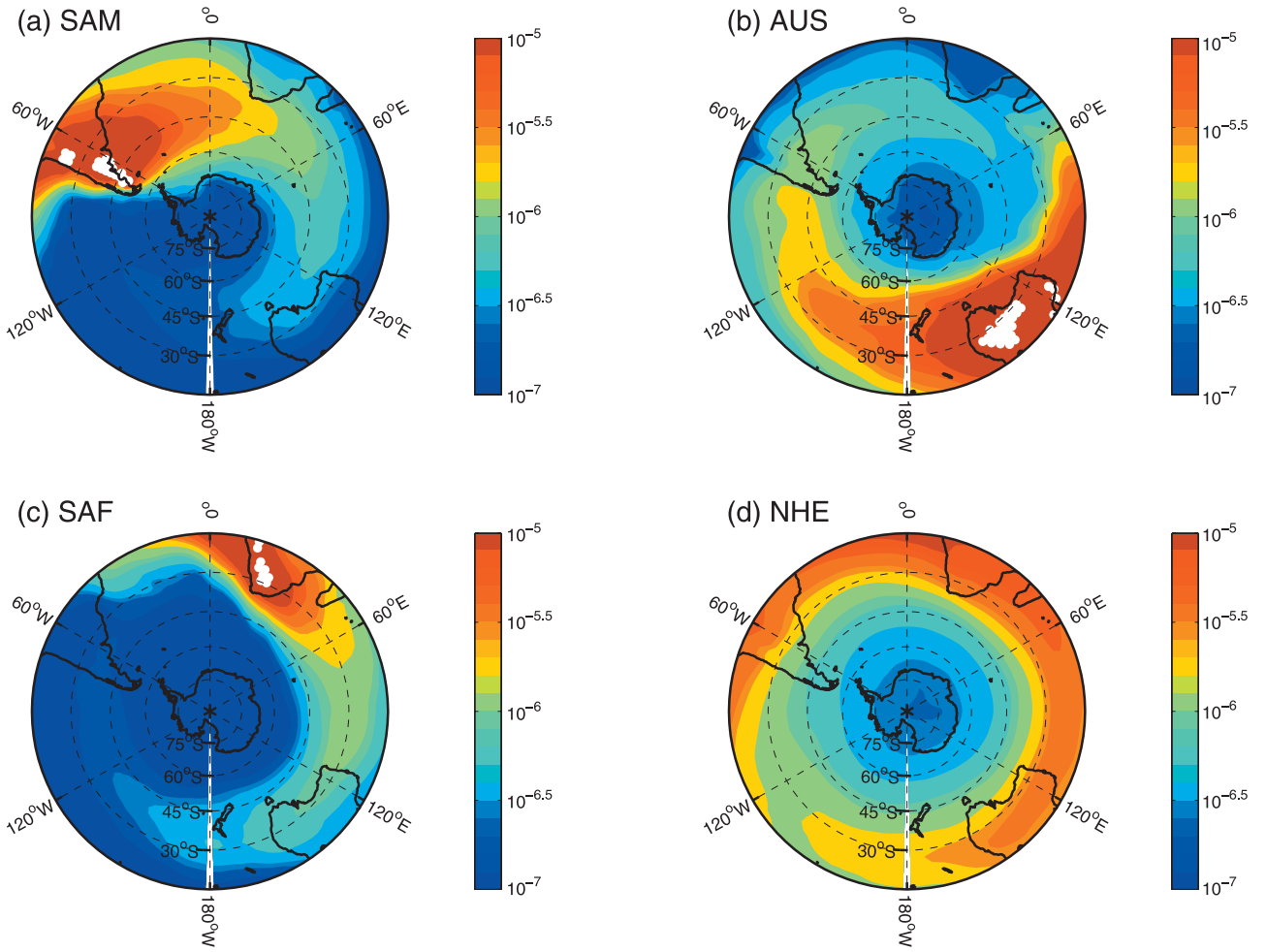

Figure 8. Annual mean atmospheric dust burden (kg m^{-2}), in the Southern Ocean and Antarctica from the four individual sources, (a) SAM, (b) AUS, (c) SAF, and (d) NHE, respectively. White dots are the corresponding source regions in SH.

tends to maintain dust in the boundary layer, but because of the strong westerlies, SAM dust may be transported over a long distance. In Australia, the mean vertical wind velocities remain mostly positive (upward) over major dust sources regions such as Lake Eyre [*McGowan et al.*, 2000], transporting dust above the boundary layer.

[41] As shown in Figures 7c and 7g, dust concentration from SAF is in upper troposphere but is about a factor of 10 lower than the other two SH sources. Since the contribution from SAF appears to be negligible, the underestimate of dust emission from SAF sources, discussed in section 2.2, should not affect our analysis of dust characteristics over the Southern Ocean and Antarctica.

[42] A distinct feature shown in Figures 7d and 7h is the meridional transport of dust from NHE, primarily from North Africa, in the upper troposphere region all the way to Antarctica which might result from the isentropic mixing and low removal of dust in this level. To our knowledge this result has never been shown before, but its validation through comparison with measurements is particularly difficult because the concentration is very low (less than 0.05 kg m^{-3}).

5.2. Atmospheric Dust Burden

[43] Figures 8a–8d illustrate the annual mean dust burden from the four principal sources, SAM, AUS, SAF, and NHE respectively. All the four figures show strong eastward transport patterns in mid and high latitude SH, especially for the three SH continental sources, as the prevailing midlatitude westerlies carry dust over a long distance [*Gassó and Stein*, 2007]. On the other hand, the dust burdens in Figure 8 do not have clear feature of southward transport in the annual mean basis since the meridional wind is relatively weak and the penetration of dust into southern polar regions is primarily on synoptic timescales [*Krinner and Genthon*, 2003].

[44] The eastward transport trend is obvious for the SAM dust features shown in Figure 8a. The burden decreases rapidly during its eastward transport, becoming one order of magnitude less before reaching South Africa and two orders less near Australia than that seen at the source. SAM dust is dominant in South Atlantic Ocean contributing more than half of the total dust burden for the entire region. It is also important in South Indian Ocean, and penetrates into the eastern coastal regions around Antarctica.

[45] Most AUS dust is transported eastward into the South Pacific Ocean, but there is also a component which goes northwest into the South Indian Ocean (Figure 8b); this is mainly from the northern and western Australian deserts [*Marx et al.*, 2005]. Because of its high emission rate (Figure 2) and rapid transport by the westerlies, the longitudinal gradient of the dust burden is less pronounced than that of SAM. The burden is still dominant near the South America's west coast and further eastward transport of AUS dust is mostly blocked by the Andes Mountains at $\sim$60°W, as seen by the reduction of mass burden along Chile in Figure 8b. In Antarctica, the burden is relatively large in the western sector facing the Pacific Ocean.

[46] SAF dust is quite localized near the source regions mostly because of the small emission magnitude and weak transport. The more northern locations of the major SAF source regions, compared with those in SAM and AUS, also contribute to the localization of SAF dust since SAF is thus far remote from the very strong influence of the westerlies. Most SAF dust sources are located at South Africa's west coast under the influence of northward winds at the eastern branch of the high pressure system over South Atlantic Ocean, as indicated by the AM2 wind and sea level pressure meteorological patterns. It prevents a prominent eastward and southward transport. Thus the SAF dust contribution to total dust burden is nearly negligible at the high SH latitudes compared with that from the other sources (Figure 8c), similar to the discussions in 3.3.1.

[47] Figure 8d shows clearly that NHE dust gets transported to the SH high latitude regions. The transport is mainly in the upper troposphere at around 200 mb. The longitudinal gradient is smaller than the other three SH continental sources, being more zonally uniformly distributed as a consequence of most of the dust being transported in the free troposphere and thereby getting mixed more uniformly. The burden is relatively higher in the South Atlantic and South Indian Oceans, but less in the South Pacific Ocean. Overall, the NHE dust accounts for $\sim$20% of the total burden in the Southern Oceans. In central Antarctica, the fractional contribution is higher, up to $\sim$40%. The total dust burden from individual source and the fractional contribution in Southern Ocean and Antarctica are summarized in Table 2.

5.3. Dust Deposition

[48] As the dust vertical profiles seem to depend on the origin, it is logical that dust deposition, including the process of deposition, would also be affected by its origin. Simulations show that, in the Southern Ocean, wet deposition is the main removal process (90% of the total removal) of the dust from AUS and NHE, because these dust particles lie in the mid and upper troposphere. In contrast, SAM dust, which lies mostly in the boundary layer, contributes relatively more via dry deposition, 25% of total removal, than in the case of AUS and NHE. In Antarctica, the dry deposition and wet deposition are comparable for dust from all the sources, except that SAM dust dry deposition is slightly higher than the wet deposition.

[49] Figures 9a–9d show the annual mean dust deposition from the four principal sources for the SH mid and high latitude regions. The magnitude of the deposition fluxes into Southern Ocean and Antarctica are summarized in Table 3.

[50] Similar to the distribution of the mass burdens, the dust originating from SAM (Figure 9a) is dominant in the deposition to the east and south of the source regions. It represents greater than 90% of the total dust deposition in the South Atlantic Ocean. AUS contributes to most of the dust deposited in the South Pacific Ocean ($\sim$ 86%), which is also to the east and south of the source (Figure 9b). SAF dust is confined to the low latitudes and is significant only in the midlatitudes in Indian Ocean near the source (Figure 9c). In contrast to the contribution to the dust burden (Figure 8), NHE dust's contribution to total deposition is quite small (Figure 9d), much less than those from AUS and SAM.

[51] In contrast to Figure 8, the distribution patterns of dust deposition in Figure 9 are not as spatially homogeneous as that of the dust burden. Extremely low deposition can be seen in inland Antarctica, central Australia, west coasts of South America and South Africa. These regions are dominated by high pressure systems most of the time during the year and are characterized by low precipitation; thus, wet deposition accounts less than 10% of the total dust deposition. This indicates an important role of precipitation on the distribution of dust deposition besides the obvious influence of the winds.

[52] Another distinct difference between dust burden and deposition in these regions is the relative contribution from NHE. SAM and AUS are the major contributors for dust deposition, while NHE's contribution is much smaller compared with that for the dust burden. This difference results from the smaller deposition rates of NHE dust compared with other sources. First, the transport of NHE dust to Southern Ocean and Antarctica is mainly through upper troposphere near the tropopause (Figure 7). Less NHE dust is washed out by precipitation leading to the low wet deposition rate in these regions. Secondly, NHE dust undergoes a very long range transport to reach the high SH latitude; during this process, the large dust particles tend to be removed. NHE dust over Antarctica consists of a relatively greater fraction of small dust particles, e.g., $\sim$ 50% from the smallest dust bin with radius 0.1–1 μm, in the simulation. Thus the corresponding dry deposition rate is also small, and the total removal for NHE dust is not as strong as that for dust from other sources although the contribution to the total dust burden of NHE is large.

[53] Relating to the discussion on the origin of dust in Antarctica in recent years from isotopic analysis [e.g., *Basile et al.*, 1997] and model simulations [*Mahowald et al.*, 1999], Figure 10 illustrates the fractional contribution of the three SH sources simulated by AM2 using the tagging method. It shows that SAM and AUS are dominant for the dust deposition in polar region, while SAF contributes a relatively small amount. NHE's contribution is small and thus not shown in this figure. The dust deposition in the half of Antarctic continent facing the Pacific Ocean is essentially from Australia, while that in the other half facing the Atlantic and Indian Oceans is mainly from South America, mostly from Patagonia.

[54] Figure 10 also indicates the contribution of different sources to the ice core site, Russian Vostok station (78°S, 106°E), which has formed the basis of many investigations on the origin of dust in the ice cores. AM2 simulations show that its location coincides approximately with the boundary separating the respective influences of SAM and AUS on

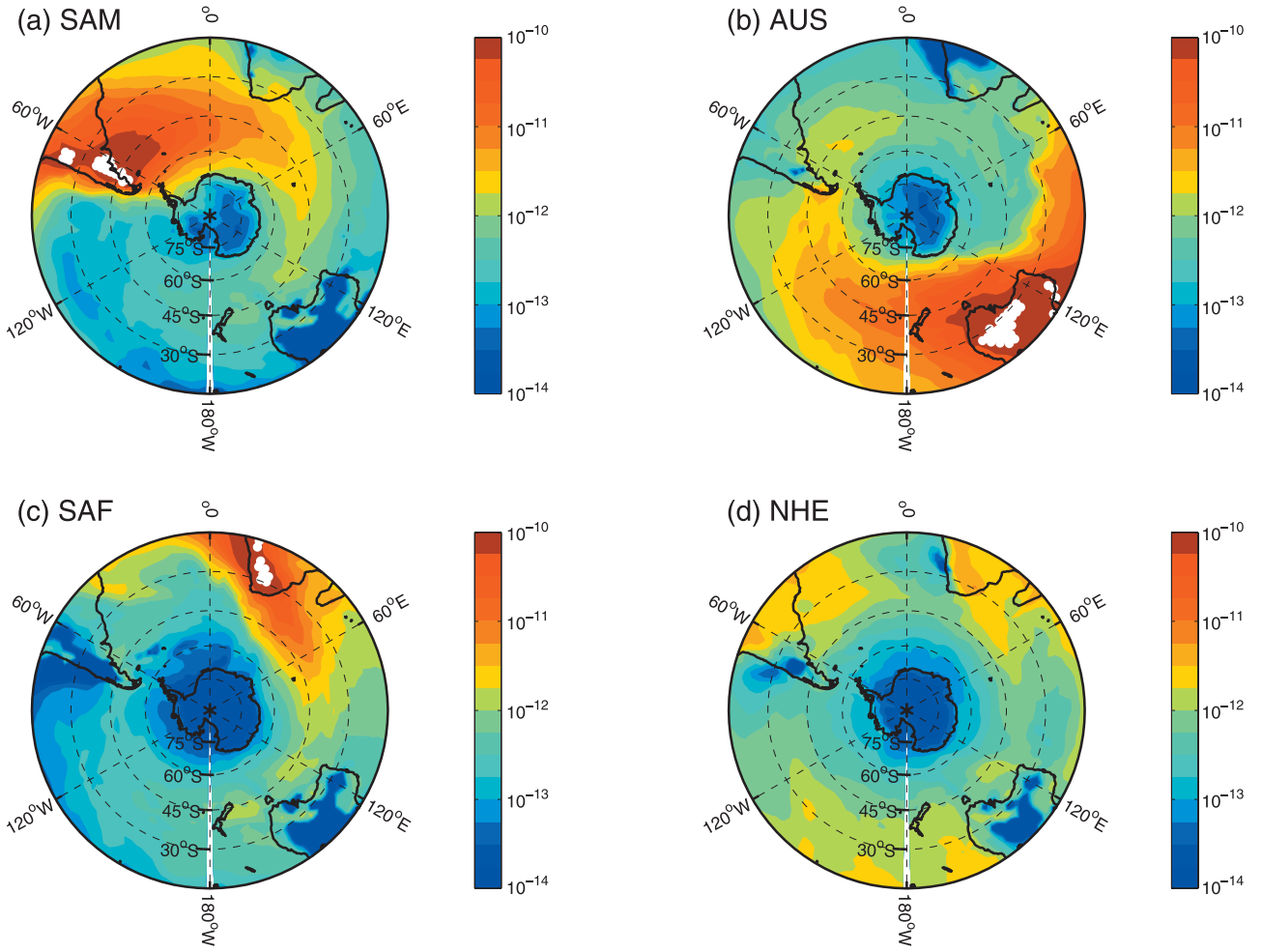

Figure 9. Annual mean dust deposition, in unit of kg m^{-2} s^{-1}, in Southern Ocean and Antarctica from the four individual sources, (a) SAM, (b) AUS, (c) SAF, and (d) NHE, respectively. White dots are the corresponding source regions in SH.

dust deposition (Figure 10) in the present climate. Quantitatively, dust depositing over Vostok site comes essentially from South America (~45%), while Australia also contributes significantly (~35%). This is in agreement with the isotopic analysis of Vostok data by *Revel-Rolland et al.* [2006] for the present climate and similar to the pattern of contribution from the source apportionment simulated by *Mahowald* [2007]. It provides another evidence on the ice core dust origin based on GCM simulations. The AM2 simulations not only quantify the dust origin for the whole Southern Ocean and Antarctica, but also show the characteristics of how the dust from each individual source is transported and deposited into these regions.

6. Discussion

[55] As this study is focused on the contribution of dust sources to the distribution and deposition of dust in the SH,

Table 3. Dust Deposition (Tg a^{-1}) and Fractional Contribution (Percentage) From Individual Sources[a]

Deposition (Tg a^{-1})	Total	SAM	AUS	SAF	NHE
South Pacific	3.59	0.22	3.07	0.11	0.17
South Atlantic	5.60	5.31	0.22	0.03	0.06
South Indian	1.11	0.64	0.23	0.16	0.07
Southern Oceans (total)	10.30	6.18 (~58%)	3.52 (~36%)	0.29 (~2%)	0.30 (~3%)
Antarctica	~0.06	~0.03 (~50%)	~0.02 (~35%)	<0.01 (~5%)	<0.01 (~10%)

[a]Note the deposition is only for 1988, which is higher than the 20-year mean value. The deposition to oceans is calculated only over ocean surfaces, and the South Pacific, Atlantic and Indian Oceans are specified as the regions south of 50°S.

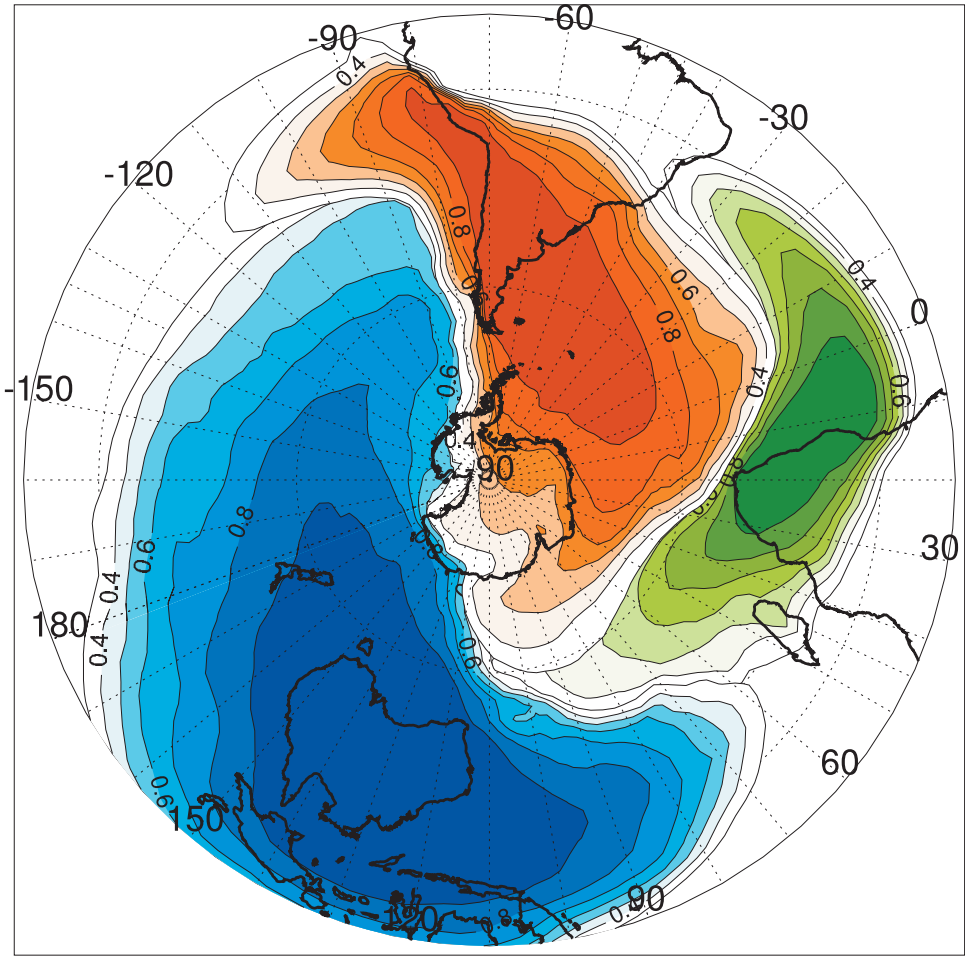

Figure 10. Relative contribution (fraction) from the three SH sources to dust deposition in high latitude SH. Only contributions larger than 30% are plotted, with the red, blue, and green shadings representing the contributions from SAM, SAF, and AUS, respectively.

and the emission parameters of equation (1) are ill-constrained by the lack of adequate data, we evaluate, in this section, the influence of these two parameters on our results.

[56] In our simulations, there is no interaction between aerosol and radiation and cloud microphysics. Therefore dust concentration and deposition are proportional to the constant C. Selecting a particular value of this parameter will change the magnitude of dust concentration and removal but not the relative contribution of each sources. As the focus on this latter point, our results are independent of C.

[57] The threshold of wind erosion, u_t, essentially shuts down the weaker sources, and as its value increases, only the sources with strong surface wind speed will be activated. If there is an important gradient of surface wind speed over the source regions, the spatial distribution of dust emission may change. A displacement of dust emission may significantly affect dust transport and, consequently, its distribution and removal. To evaluate the possible effects on our results, we have performed a simulation with $u_t = 3$ m s^{-1} and C five times its original value, which offers a reasonable range in the parametric values.

[58] The results of the sensitivity study are that the global dust emission is reduced by less than 10%. The distribution of major sources has the same spatial distribution in the SH compared to the standard simulation. The surface dust concentration pattern does not change much between the two simulations. The correlation coefficient of surface concentrations between the simulated values in the sensitivity test and observations is 0.95. It is slightly smaller than that in Figure 4. Differences exist mainly for the sites in the Northern Hemisphere. The dust transported across the equator from Northern Hemisphere increases by 3 Tg a^{-1} in the sensitivity test, while the differences in the emission, transport, and deposition in SH, compared with the standard simulation (Figure 3), is mostly less than 20%. The sensitivity test did not change the vertical distributions, which include the same maxima as shown in Figure 6: one near the surface at ~60°W and the other centered at ~700 mb (~160°–180°E) in the Southern Ocean. In Antarctica, the maximum dust concentration is again located in the upper troposphere (near the tropopause) between 400–200 mb. The sensitivity study basically shows that our main conclusions are not affected greatly by the choice of the values for C and u_t. We may have anticipated this lack of sensitivity to u_t as dust sources in Patagonia are swept by strong winds, and dust plumes out of Australia are caused by intense winds along cold fronts. In both cases, the winds are high enough to be well above the possible choice of the

value u_t. Furthermore, the methodology used by *Prospero et al.* [2002] to determine dust sources, and that used by *Ginoux et al.* [2001] to build their source function S, tends to discard weaker sources and only the most frequent dust plumes are taken into account. Thus it may be possible that the S function contains implicitly some information on the wind conditions.

7. Conclusion

[59] This work presents results from simulations using the GFDL state-of-the-art Atmospheric General Circulation Model AM2. It represents a modeling attempt to quantify the contributions from the different continental sources by tagging dust according to its origin. We evaluate the contribution of each source to the emission, distribution of concentration, mass burden and deposition of dust in the Southern Ocean and Antarctica, and show that each source produces distinctive meridional transport, vertical distribution, and deposition patterns. The dust in SH is primarily from Australia (120 Tg a^{-1}), Patagonia (38 Tg a^{-1}) and the inter-hemispheric transport from Northern Hemisphere (31 Tg a^{-1}). A small fraction of it is transported and deposited in the Southern Ocean and Antarctica (7 Tg a^{-1}). The dust in the high SH latitude atmosphere can be partitioned in terms of the contributions from the four principal source regions, distinctive vertical profiles, meridional transport and deposition. Overall, mineral dust is distributed throughout the troposphere, but the boundary layer, mid-troposphere and upper troposphere are dominated by dust from SAM, AUS and NHE, respectively.

[60] Due to the prevailing westerlies, the distributions of dust burden and deposition show the eastward transport trend for dust from the principal sources. SAF's contribution to both dust burden and deposition in Southern Ocean and Antarctica are negligible. The model indicates that NHE's contribution to atmospheric burden in Antarctica can reach ~40%, despite the fact that its deposition is small. This could have important implications for ozone photochemistry but we could not find any data sensitive enough to measure the low concentrations of the dust in the upper troposphere to confirm our results. SAM and AUS contribute about equally to the total dust burden and deposition in Southern Ocean and Antarctica, essentially to the east of the two continents. They combine to contribute more than 85% of the dust deposition over the Southern Ocean and Antarctica continent, but have substantially lower contribution (totally ~50–70%) to atmospheric burden in these regions. This difference results from the smaller deposition rates of NHE dust compared to the other sources.

[61] The present simulations show that South America and Australia are the two main sources of the dust deposition in both Southern Ocean and Antarctica, but they differ zonally with each one dominating half of a hemisphere along 120°E – 60°W: the half comprising the Atlantic and Indian oceans in the case of South American dust and the Pacific half in the case of the Australian dust. The model also quantifies the origin of dust over Antarctica such as those over ice core sites. For instance, the location of Vostok station is close to the boundary of SAM and AUS dominant regions for dust deposition (45% from SAM and 35% from AUS). Since the long record of dust concentration in ice cores in Antarctica (e.g., Vostok ice cores) provides a unique data set to study long-term climate change, identifying the origin of dust in these ice cores could have implication in explaining the increased dust concentration during the LGM, understanding the role of dust in climate change between glacial and inter-glacial periods, and constraining model simulations of dust for different climates. However, since there could be a shift in the origin of dust between the Holocene and Pleistocene [*Revel-Rolland et al.*, 2006], more studies especially GCM simulations on past climate would be necessary to improve our understanding on these issues.

[62] **Acknowledgments.** We would like to thank Joseph Prospero, University of Miami, for providing us with the measured dust concentrations at the surface. We also thank the reviewers who helped to improve the quality of this paper.

References

Basile, I., F. E. Grousset, M. Revel, J. R. Petit, P. E. Biscaye, and N. I. Barkov (1997), Patagonian origin of glacial dust deposited in East Antarctica (Vostok and Dome C) during glacial stages 2, 4 and 6, *Earth Planet. Sci. Lett.*, *146*, 573–589.

Boucher, O., M. Pham, and C. Venkataraman (2002), Simulation of the atmospheric sulfur cycle in the Laboratoire de Meteorologie Dynamique general circulation model: Model description, model evaluation, and global and European budgets, *Note Sci. de l'IPSL*, *23*, 27.

Cakmur, R. V., R. L. Miller, J. Perlwitz, I. V. Geogdzhayev, P. Ginoux, D. Koch, K. E. Kohfeld, I. Tegen, and C. S. Zender (2006), Constraining the magnitude of the global dust cycle by minimizing the difference between a model and observations, *J. Geophys. Res.*, *111*, D06207, doi:10.1029/2005JD005791.

DeFries, R. S., and J. R. G. Townshend (1994), NDVI-derived land cover classification at global scales, *Int. J. Remote Sens.*, *15*, 3567–3586.

Delmonte, B., I. Basile-Doelsch, J. R. Petit, V. Maggi, M. Rolland-Revel, A. Michard, E. Jagoutz, and F. Grousset (2004), Comparing the EPICA and Vostok dust records during the last 220,000 years: Stratigraphical correlation and origin in glacial periods, *Earth Sci. Rev.*, *66*, 63–87.

Dentener, F. J., G. R. Carmichael, Y. Zhang, J. Lelieveld, and P. J. Crutzen (1996), Role of mineral aerosol as a reactive surface in the global troposphere, *J. Geophys. Res.*, *101*, 22,869–22,889.

Fan, S.-M., W. J. Moxim, and H. Levy II (2006), Aeolian input of bioavailable iron to the ocean, *Geophys. Res. Lett.*, *33*, L07602, doi:10.1029/2005GL024852.

Gaiero, D. M., J. L. Probst, P. J. Depetris, S. M. Bidart, and L. Leleyter (2003), Iron and other transition metals in Patagonian riverborne and windborne materials: Geochemical control and transport to the southern South Atlantic Ocean, *Geochim. Cosmochim. Acta*, *67*(19), 3603–3623.

Gassó, S., and A. F. Stein (2007), Does dust from Patagonia reach the sub-Antarctic Atlantic Ocean?, *Geophys. Res. Lett.*, *34*, L01801, doi:10.1029/2006GL027693.

Gaudichet, A., M. De Angelis, R. Lefevre, J. R. Petit, Y. S. Korotkevitch, and V. N. Petrov (1992), Comments on the origin of dust in East Antarctica for present and ice age conditions, *J. Atmos. Chem.*, *14*, 129–142.

Genthon, C. (1992), Simulations of desert dust and sea-salt aerosols in Antarctica with a general circulation model of the atmosphere, *Tellus, Ser. B*, *44*, 371–389.

GFDL Global Atmospheric Model Development Team (2004), The new GFDL global atmosphere and land model AM2-LM2: Evaluation with prescribed SST simulations, *J. Clim.*, *17*, 4641–4673.

Ginoux, P., M. Chin, I. Tegen, J. M. Prospero, B. Holben, O. Dubovik, and S. Lin (2001), Sources and distributions of dust aerosols simulated with the GOCART model, *J. Geophys. Res.*, *106*(D17), 22,055–22,074.

Grousset, F. E., P. E. Biscaye, M. Revel, J. R. Petit, K. Pye, S. Joussaume, and J. Jouzel (1992), Antarctic (Dome C) ice-core dust at 18 k.y. B. P.: isotopic constraints on origins, *Earth Planet. Sci. Lett.*, *111*, 175–182.

Hsu, N. C., S. C. Tsay, M. D. King, and J. R. Herman (2004), Aerosol properties over bright-reflecting source regions, *IEEE Trans. Geosci. Remote Sens.*, *42*, 557–569.

Kohfeld, K. E., and S. P. Harrison (2001), DIRTMAP: The geological record of dust, *Earth Sci. Rev.*, *54*, 81–114.

Krinner, G., and C. Genthon (2003), Tropospheric transport of continental tracers towards Antarctica under varying climatic conditions, *Tellus, Ser. A and Ser. B*, *55B*, 54–70.

Labraga, J. C. (1994), Extreme winds in the Pampa-Del-Castillo Plateau, Patagonia, Argentina, with reference to wind farm settlement, *J. Appl. Meteorol.*, *33*(1), 85–95.

Lin, S.-J. (2004), A "vertically Lagrangian" finite-volume dynamical core for global models, *Mon. Weather Rev.*, *132*(10), 2293–2307.

Lunt, D. J., and P. J. Valdes (2002), Dust deposition and provenance at the Last Glacial Maximum and present day, *Geophys. Res. Lett.*, *29*(22), 2085, doi:10.1029/2002GL015656.

Luo, C., N. Mahowald, and J. del Corral (2003), Sensitivity study of meteorological parameters on mineral aerosol mobilization, transport, and distribution, *J. Geophys. Res.*, *108*(D15), 4447, doi:10.1029/2003JD003483.

Luo, C., N. Mahowald, and C. Jones (2004), Temporal variability of dust mobilization and concentration in source regions, *J. Geophys. Res.*, *109*, D20202, doi:10.1029/2004JD004861.

Mahowald, N. M. (2007), Anthropocene changes in desert area: Sensitivity to climate model predictions, *Geophys. Res. Lett.*, *34*, L18817, doi:10.1029/2007GL030472.

Mahowald, N., K. Kohfeld, M. Hansson, Y. Balkanski, S. P. Harrison, I. C. Prentice, M. Schulz, and H. Rodhe (1999), Dust sources and deposition during the last glacial maximum and current climate: A comparison of model results with paleodata from ice cores and marine sediments, *J. Geophys. Res.*, *104*(D13), 15,895–15,916.

Mahowald, N. M., R. G. Bryant, J. del Corral, and L. Steinberger (2003), Ephemeral lakes and desert dust sources, *Geophys. Res. Lett.*, *30*(2), 1074, doi:10.1029/2002GL016041.

Mahowald, N. M., D. R. Muhs, S. Levis, P. J. Rasch, M. Yoshioka, C. S. Zender, and C. Luo (2006), Change in atmospheric mineral aerosols in response to climate: Last glacial period, preindustrial, modern, and doubled carbon dioxide climates, *J. Geophys. Res.*, *111*, D10202, doi:10.1029/2005JD006653.

Martin, J. M. (1990), Glacial-interglacial CO2 change: The Iron hypothesis, *Paleoceanography*, *5*, 1–13.

Marx, S. K., B. S. Kamber, and H. A. McGowan (2005), Estimates of Australian dust flux into New Zealand: Quantifying the eastern Australian dust plume pathway using trace element calibrated 210Pb as a monitor, *Earth Planet. Sci. Lett.*, *239*, 336–351.

McConnell, J. R., A. J. Aristarain, J. R. Banta, P. R. Edwards, and J. C. Simoes (2007), 20th-Century doubling in dust archived in an Antarctica Peninsula ice core parallels climate change and desertification in South America, *Proc. Natl. Acad. Sci. U.S.A.*, *104*, 5743.

McGowan, H. A., G. H. McTainsh, P. Zawar-Reza, and A. P. Sturman (2000), Identifying regional dust transport pathways: Application of kinematic trajectory modeling to a trans-Tasman case, *Earth Surf. Processes Landforms*, *25*(6), 633–647.

McTainsh, G. H. (1998), Dust storm index, sustainable agriculture: Assessing Australia's recent performance. A report of the national colllaborative project on indicators for sustainable agriculture, *SCARM Tech. Rep.*, *70*, 6572.

McTainsh, G. H., and A. W. Lynch (1996), Quantitative estimates of the effect of climate change on dust storm activity in Australia during the Last Glacial Maximum, *Geomorphology*, *17*, 263–271.

Moorthi, S., and M. J. Suarez (1992), Relaxed Arakawa-Schubert. A Parameterization of moist convection for general circulation models, *Mon. Weather Rev.*, *120*, 978–1002.

Pereira, E. B., A. W. Setzer, and I. F. A. Cavalcanti (1988), Radon-222 in the Antarctic Peninsula during 1986, *Radiat. Prot. Dosimetry*, *24*(1/4), 85–88.

Petit, J. R., et al. (1999), Climate and atmospheric history of the past 420,000 years from the Vostok ice core, Antarctica, *Nature*, *399*, 429–436.

Polian, G., G. Lamert, B. Ardouin, and A. Jegou (1986), Long-range transport of continental radon in subantarctic and Antarctica areas, *Tellus, Ser. A and Ser. B*, *38B*, 178–189.

Prospero, J. M. (1996), The atmospheric transport of particles to the ocean, in *Particle Flux in the Ocean*, vol. 57, edited by V. Ittekkot et al., *SCOPE*, *57*, 19–52.

Prospero, J. M., P. Ginoux, O. Torres, and S. Nicholson (2002), Environmental characterization of global sources of atmospheric soil dust derived from the NIMBUS 7 Total Ozone Mapping Spectrometer (TOMS) absorbing aerosol product, *Rev. Geophys.*, *40*(1), 1002, doi:10.1029/2000RG000095.

Ramaswamy, V., O. Boucher, J. Haigh, D. Hauglustane, J. Haywood, G. Myhre, T. Nakajima, G. Y. Shi, and S. Solomon (2001), Radiative forcing of climate change, in *Climate Change 2001: The Scientific Basis*, chap. 6, edited by J. T. Houghton et al., pp. 349–416, Cambridge Univ. Press, Cambridge.

Ramonet, M., J. C. Le Roulley, P. Bousquet, and P. Monfray (1996), Radon-222 measurements during the Tropoz II campaign and comparison with a global atmospheric transport model, *J. Atmos. Chem.*, *23*, 107–136.

Revel-Rolland, M., P. De Deckker, B. Delmonte, P. P. Hesse, J. W. Magee, I. Basile-Doelsch, F. Grousset, and D. Bosch (2006), Eastern Australia: A possible source of dust in East Antarctica interglacial ice, *Earth Planet. Sci. Lett.*, *249*, 1–13.

Rosenfeld, D., Y. Rudich, and R. Lahav (2001), Desert dust suppressing precipitation: A possible desertification feedback loop, *Proc. Natl. Acad. Sci. U.S.A.*, *98*, 5975.

Slinn, W. G. N. (1982), Prediction for particle deposition to vegetative surfaces, *Atmos. Environ.*, *16*, 1785–1794.

Steffensen, J. P. (1997), The size distribution of microparticles from selected segments of the Greenland Ice Core Project ice core representing different climatic periods, *J. Geophys. Res.*, *102*(C12), 26,755–26,763.

Torres, O., P. K. Bhartia, J. R. Herman, A. Sinyuk, P. Ginoux, and B. Holben (2002), A long-term record of aerosol optical depth from TOMS observations and comparison to AERONET measurements, *J. Atmos. Sci.*, *59*, 398–413.

Watson, A. J., D. C. E. Bakker, A. J. Ridgwell, P. W. Boyd, and C. S. Law (2000), Effect of iron supply on Southern Ocean CO2 uptake and implications for glacial atmospheric CO2, *Nature*, *407*, 730–733.

Werner, M., I. Tegen, S. P. Harrison, K. E. Kohfeld, I. C. Prentice, Y. Balkanski, H. Rodhe, and C. Roelandt (2002), Seasonal and interannual variability of the mineral dust cycle under present and glacial climate conditions, *J. Geophys. Res.*, *107*(D24), 4744, doi:10.1029/2002JD002365.

P. Ginoux and V. Ramaswamy, Geophysical Fluid Dynamics Laboratory, NOAA, 201 Forrestal Road, Princeton, NJ 08540, USA.

F. Li, Program in Atmospheric and Oceanic Sciences, Princeton University, 308B GFDL, 201 Forrestal Road, Princeton, NJ 08540, USA. (fuyuli@princeton.edu)